

Abstract

The development of atmospheric parameterizations based on neural networks is often hampered by numerical instability issues. Previous attempts to replicate these issues in a toy model have proven ineffective. We introduce a new toy model for atmospheric dynamics, which consists in an extension of the Lorenz'63 model to a higher dimension. While neural networks trained on a single orbit can easily reproduce the dynamics of the Lorenz'63 model, they fail to reproduce the dynamics of the new toy model, leading to unstable trajectories. Instabilities become more frequent as the dimension of the new model increases, but are found to occur even in very low dimension. Training the neural network on a different learning sample, based on Latin Hypercube Sampling, solves the instability issue. Our results suggest that the design of the learning sample can significantly influence the stability of dynamical systems driven by neural networks.

Plain Language Summary

Part of atmospheric models accounting for small-scale processes, called parameterizations, can be developed by using artificial intelligence techniques, such as neural networks. The development of such parameterizations is often hampered by numerical instability issues. Toy models commonly used in atmospheric research are not complex enough to allow the study of these instabilities, and are easily learnt by neural networks. Here, we introduce a new toy model for atmospheric dynamics, which consists in an extension of the famous Lorenz'63 model to a higher dimension. While neural networks trained on a single orbit can easily reproduce the Lorenz'63 model, they fail to replicate the new toy model, leading to unstable trajectories. Training the neural network on a specifically designed learning sample, which explores the full phase space in the neighborhood of a given trajectory, solves the instability issues. Our results suggest that the design of the learning sample can significantly influence the stability of dynamical systems driven by neural networks.

1 Introduction

Many efforts have been made over the last few years to develop new, data-driven parameterization schemes using artificial intelligence (AI) for use in atmospheric models (e.g. Gentine et al., 2018; O'Gorman & Dwyer, 2018; Brenowitz & Bretherton, 2018). Even though they promise numerically affordable yet accurate physics for low resolution

42 atmospheric models (e.g. climate models), current state-of-the-art AI parameterizations
43 are still biased and, more importantly, they face numerical instability issues. As reported
44 by Rasp (2020), neural networks (NNs) are often numerically unstable, when coupled
45 to the large-scale atmospheric fluid mechanics solver (e.g. Rasp et al., 2018; Brenowitz
46 & Bretherton, 2019). Parameterizations based on random forests (RF) have been reported
47 to be stable (Yuval & O’Gorman, 2020). But, when compared offline, NN-based param-
48 eterizations seem to outperform RF-based parameterizations (Brenowitz, Henn, et al., 2020).

49 Stability issues can be interpreted as a result of breaking physical laws, and some
50 authors propose techniques to ensure compliance with these laws (e.g. Beucler et al., 2019).
51 Brenowitz, Beucler, et al. (2020) shows that instabilities are related to the linearized be-
52 havior of NNs when coupled to idealized wave dynamics. To fix numerical instabilities,
53 Rasp (2020) proposes a coupled online learning method where a NN model, which was
54 first trained offline, is continuously corrected according to online prediction errors. This
55 concept is illustrated using the Lorenz’96 model (Lorenz, 1996).

56 Lorenz’96 (hereafter L96) and Lorenz’63 (Lorenz, 1963, hereafter L63) models of-
57 ten serve as toy models for atmospheric modeling, drawing simplified versions of the at-
58 mospheric flow. They have been extensively used as a test bed for assessing the use of
59 data-driven methods in atmospheric models. L63 model has been accurately learnt by
60 feedforward neural networks (Scher & Messori, 2019) or reservoir networks (Pathak et
61 al., 2017). L96 dynamics has also been accurately learnt by feedforward NNs, recurrent
62 NNs or generative adversarial networks (Dueben & Bauer, 2018; Chattopadhyay et al.,
63 2020; Gagne et al., 2020), without reporting stability issues. Both L63 and L96 toy mod-
64 els appears to be insufficiently complex to study numerical instabilities encountered with
65 more complex systems.

66 Understanding the instability encountered in the development of data-driven pa-
67 rameterizations is of outmost importance for any climate application. However, no toy
68 model for atmospheric dynamics is currently available to investigate such instability is-
69 sues. The first aim of this paper is to introduce a toy model for atmospheric dynamics,
70 consisting in a higher dimensional version of L63, which exhibits instability when learnt
71 by a NN. The second objective is to propose a possible method to ensure stability of the
72 NN-generated trajectories, which in our case involves using a specific learning sample.
73 Both objectives can be seen as steps towards solving numerical instabilities – an issue

74 which remains challenging to develop suitable NN-based parameterizations for atmospheric
75 models.

76 Section 2 describes the Lorenz'63 model and illustrates that this model is not com-
77 plex enough to challenge NNs. In Section 3, we introduce the embedded Lorenz'63 model,
78 and show that learning of this simple model with NNs leads to unstable trajectories. In
79 Section 4, a method to address these instability issues is proposed. Finally, conclusions
80 and discussions will be drawn in Section 5.

81 **2 Learning the Lorenz'63 model**

82 By expanding the set of partial differential equations of Rayleigh-Bénard convec-
83 tion into Fourier series and then truncating, Lorenz (1963) derives a finite system of or-
84 dinary differential equations, given by:

$$\begin{aligned} \dot{x}_1 &= \sigma(x_2 - x_1), \\ \dot{x}_2 &= x_1(\rho - x_3) - x_2, \\ \dot{x}_3 &= x_1x_2 - \beta x_3 + x_1. \end{aligned} \tag{1}$$

85 The evolution of the state variable $\mathbf{x} = (x_1, x_2, x_3)$ is governed by the set of parame-
86 ters (σ, ρ, β) . L63 admits a chaotic solution for some values of these parameters, in par-
87 ticular $\sigma = 10$, $\rho = 28$ and $\beta = 8/3$. We use these values in the following. Although
88 computationally cheap, L63 is able to mimic some properties of the atmospheric flow.
89 Hence, it is a suitable toy model to perform proof-of-concept experiments.

90 Recently, the L63 model has been used as a test bed for assessing the use of data-
91 driven methods in atmospheric models. The system of equations (1) can be formally rewrit-
92 ten:

$$\dot{\mathbf{x}}(t) = f(\mathbf{x}(t)). \tag{2}$$

93 Data-driven methods provide an approximate function, \hat{f} , to replace the 'true' function
94 f , and thus they replace the initial dynamical system by:

$$\dot{\mathbf{x}}(t) = \hat{f}(\mathbf{x}(t)). \tag{3}$$

95 That is, learning a dynamical system usually involves learning its derivative. For the L63
96 model specifically, various functions \hat{f} have been proposed recently, e.g., using sparse lin-
97 ear regression (Brunton et al., 2016), feedforward neural networks (Scher & Messori, 2019),
98 or reservoir networks (Pathak et al., 2017). Fitting \hat{f} always involves an optimization

99 over a set of free parameters θ . This optimization is done for a given loss function, and
 100 a given learning sample. In the case of dynamical systems, the learning sample is typ-
 101 ically a time series, also called an *orbit*, obtained by numerical integration of the system,
 102 e.g., Eq. (2). We note $[\mathbf{x}^{orb}]$ this learning sample:

$$[\mathbf{x}^{orb}] = \{(\mathbf{x}^n, f(\mathbf{x}^n))\}_{n=1..N}, \quad (4)$$

103 where \mathbf{x}^n denotes the state of the system, $\mathbf{x}(t_n)$, at time t_n .

104 To learn the L63 model, we use one single orbit as a learning sample. This orbit
 105 is obtained by integrating Eqs. (1) with a time-step of $\Delta t = 0.05$ using a fourth-order
 106 Runge-Kutta time stepping scheme. The numerical integration is performed over 500 model
 107 time units (MTU, where $1 \text{ MTU} = 20 \Delta t$). Thus, the learning sample contains $N = 10000$
 108 individuals. A simple, eight-layer feedforward artificial neural network is trained to de-
 109 rive \hat{f} , using the mean squared error as the loss function. The integration of both the
 110 L63 model (Eq. 2) and its NN-approximation (Eq. 3), starting from the same initial con-
 111 dition, shows a good agreement (Fig. 1). In particular, the NN-based model does not
 112 manifest any unstable behavior, i.e., its orbits always lay on the Lorenz 'butterfly' at-
 113 tractor. Repeating this analysis with different initial conditions and/or different learn-
 114 ing samples leads to the same conclusion. This result suggests that the L63 model is not
 115 challenging enough to data-driven methods and does not allow to study instability is-
 116 sues, as previously shown in similar studies.

117 L96 provides another simple framework to study data-driven methods in the con-
 118 text of atmospheric modeling. L96 is designed to be more complex than L63, owing to
 119 its larger number of state variables. However, reservoir computers and neural networks
 120 have succeeded in learning this system without reporting instability issues. Hence, both
 121 L63 and L96 appears to be too simple to encounter the typical instability issues that still
 122 hamper the development of AI parameterizations.

123 **3 The embedded Lorenz'63 model**

124 Building a higher dimensional model on the basis of L63 has already been proposed.
 125 Musielak and Musielak (2009) added a fourth spatial variable to extend L63 equations.
 126 Champion et al. (2019) created a high-dimensional model on the basis of L63 system by
 127 using Legendre polynomials. Here, we propose a different extension of this model specif-
 128 ically designed to investigate instability issues.

129 The key idea is as follows: the standard L63 model, which is of dimension 3, is em-
 130 bedded into a larger space of dimension $d > 3$. In the selected 3-D subspace, the chaotic
 131 dynamics of L63 is kept unchanged. Any deviation from this 3-D subspace is brought
 132 back by a restoring force. We call 'embedded' L63 model (hereafter, eL63) this new sim-
 133 ple model. A formal definition of eL63 is in two steps (see Figure 2).

134 (1) Embedding: we construct a vector $\mathbf{z} = (z_1, z_2, \dots, z_d) \in \mathbb{R}^d$, and define its dy-
 135 namics by:

$$\begin{aligned} \dot{z}_1 &= \sigma(z_2 - z_1), \\ \dot{z}_2 &= z_1(\rho - z_3) - z_2, \\ \dot{z}_3 &= z_1 z_2 - \beta z_3 + z_1, \\ \dot{z}_j &= -\kappa z_j, \quad \forall j > 3. \end{aligned} \tag{5}$$

136 The first three equations are identical to L63, while the $d - 3$ additional equa-
 137 tions are simple restoring forces. For the sake of simplicity, the relaxation coef-
 138 ficient, κ , is unique. In the following, we use $\kappa = 1$. We denote \mathcal{B}_z the basis of
 139 vector \mathbf{z} .

140 (2) Random rotation: We apply a random rotation to derive the state vector of the
 141 eL63 system, $\mathbf{x} = (x_1, x_2, \dots, x_d)$:

$$\mathbf{x}(t) = P\mathbf{z}(t), \tag{6}$$

142 where $P \in \mathbb{R}^{d \times d}$ is the rotation matrix between \mathcal{B}_z and \mathcal{B}_x , the basis of \mathbf{x} . Note
 143 that the rotation matrix P does not depend on time.

144 A key property of eL63 is that $z_{j,j>3}$ exponentially decays towards zero and so $\mathbf{x}(t)$
 145 is confined within a subspace of dimension 3. This subspace can be interpreted as re-
 146 sulting, e.g., from physical but unknown constraints. The difficulty for a data-driven method
 147 to fully capture the dynamics of eL63 comes from the fact that any orbit is very thin –
 148 almost all points are located in a subspace of dimension 3. If such an orbit is used as a
 149 learning sample, any deviation from this specific subspace in a predicted trajectory can
 150 lead to an out-of-sample issue.

151 We now consider the problem of learning eL63, in the same way as done for L63
 152 in the previous section. A learning sample $[\mathbf{x}^{orb}]$ is built by integrating eL63 equations
 153 over 500 MTUs, with a timestep of $\Delta t = 0.05$ using a fourth-order Runge-Kutta scheme.
 154 The initial condition is sampled from an eL63 orbit, which is equivalent to removing the

155 model spin-up from the learning dataset, ensuring that $z_{j,j>3} \approx 0$. Therefore, the learn-
 156 ing dataset contains $N = 10000$ individuals. Both the input and the target variables
 157 are then normalized so that their mean value equals 0 and their standard deviation equals
 158 1. They are randomly partitioned into training and testing datasets, with proportions
 159 80% and 20%, respectively. A simple feedforward NN is trained to best approximate f .
 160 The NN is eight layers deep and of similar complexity to the NN that has been utilized
 161 to learn the L63 dynamics in Section 2. All layers are activated by Rectified Linear Unit
 162 (ReLU) function. With an embedding dimension $d = 4$, this neural network has 176458
 163 free parameters to fit. Learning is performed over 50 epochs, with Keras implementa-
 164 tion of Adam optimizer, parameterized with a initial learning rate of 0.001. During train-
 165 ing, the determination coefficient R^2 over the test subset is monitored. The training loss
 166 function \mathcal{L} is the mean squared error:

$$\mathcal{L}(\theta, [\mathbf{x}^{\text{train}}]) = \frac{1}{N} \sum_{n=1}^N \left\| \hat{f}_{\theta}(\mathbf{x}^n) - f(\mathbf{x}^n) \right\|^2, \quad (7)$$

167 where $[\mathbf{x}^{\text{train}}]$ denotes the training dataset, N the size of the training dataset, $\mathbf{x}^n \in [\mathbf{x}^{\text{train}}]$
 168 for $1 \leq n \leq N$, and θ denotes the set of parameters over which the optimization is
 169 made. As the learning sample consists of a single orbit, we note \hat{f}_{orb} the estimated func-
 170 tion, i.e.:

$$\hat{f}_{orb} = \hat{f}_{\theta^*} \text{ with } \theta^* = \underset{\theta}{\operatorname{argmin}} \mathcal{L}(\theta, [\mathbf{x}^{orb}]). \quad (8)$$

171 Learning is very efficient, as we get $R^2 = 0.9998$, i.e., an overall performance con-
 172 sistent with L63. To assess the stability of the trajectories generated by using \hat{f}_{orb} in-
 173 stead of f , we take an initial condition within the original learning sample $[\mathbf{x}^{orb}]$. Then,
 174 we generate the ANN-based trajectories starting from these points over 1000 MTUs, and
 175 compared them with the true eL63 orbits (i.e., integrating eL63 equations from the same
 176 initial condition). This seems long enough for a model to manifest numerical instabil-
 177 ities. Stability of the resulting orbit is assessed using a 'stability criterion' defined as fol-
 178 lows: for each $i = 1..d$, we compute the minimum (m_i) and maximum (M_i) values of
 179 x_i over the training orbit $[\mathbf{x}^{orb}]$. A N -step trajectory is considered as stable if it remains
 180 within 7 times this range of values, i.e.:

$$m_i - 3(M_i - m_i) \leq x_i^n \leq M_i + 3(M_i - m_i), \quad \forall 1 \leq i \leq d, \quad \forall 1 \leq n \leq N. \quad (9)$$

181 The choice of this stability criterion is partly arbitrary, but it is motivated by its sim-
 182 plicity.

183 The above described validation strategy is iterated over 100 different \hat{f}_{orb} , each be-
 184 ing trained with a different rotation matrix P and a corresponding learning sample $[\mathbf{x}^{orb}]$.
 185 The resulting functions \hat{f}_{orb} are then tested by generating orbits of length 1000 MTU
 186 from 30 different initial conditions sampled randomly from their respective training or-
 187 bit. As a result, stability can be assessed over 3000 simulated orbits of length 1000 MTU
 188 each. Figure 3 shows the percentage of stable trajectories generated with \hat{f}_{orb} for dif-
 189 ferent values of d , the dimension of eL63. Even with minimal embedding (i.e., $d = 4$),
 190 40% of the NN-generated orbits are unstable. With $d \geq 7$, all generated orbits are un-
 191 stable regarding the stability criterion defined by Eq. (9). The accumulation of small pre-
 192 diction errors gradually leads the NN-generated orbit away from the learning sample,
 193 in a region where \hat{f}_{orb} is not accurate. Hence, many NN-generated orbits are unstable,
 194 proving that eL63 is a very simple model (as its dimension remains very low) which is
 195 able to reproduce instability issues. Lastly, we notice that the same recipe (i.e., embed-
 196 ding) can be applied to even simpler non-chaotic dynamical system, and leads to sim-
 197 ilarly unstable trajectories when learnt by NNs (see Supplementary Information).

198 **4 Stabilizing the NN-based embedded Lorenz'63 model**

199 We now propose to illustrate a possible method to solve instability issues encoun-
 200 tered by simple NN models in the case of the eL63 model. We generate a new learning
 201 sample by taking points away from a typical orbit, taking advantage of the fact that the
 202 value of f can be sampled at any location. In this way, we better approximate the func-
 203 tion f on regions away from the eL63 attractors. This method can be thought as a data
 204 augmentation technique. Pan and Duraisamy (2018) yet proposes data augmentation
 205 as a remedy to tackle instability issues encountered in the dynamical system they study.

206 Here, we use a Latin Hypercube Sampling (LHS) (McKay, 1992) to generate a new
 207 learning sample of size $N = 10000$ (i.e., N is kept unchanged). LHS generates an op-
 208 timal near-random sample in a high-dimensional (here, dimension d) hypercube. The bound-
 209 aries of the LHS are set to 1.5 times the range of an orbit $[\mathbf{x}^{orb}]$. This calculation is done
 210 for each $i = \{1, \dots, d\}$, leading to an hypercube in the basis \mathcal{B}_x . Finally, we generate
 211 the target variables by simply applying f to the selected points, and obtain a new learn-
 212 ing sample $[\mathbf{x}^{LHS}]$. The next step is to estimate f from $[\mathbf{x}^{LHS}]$. Consistent with the pre-
 213 vious section, train and test datasets are obtained by randomly partitioning the learn-
 214 ing sample in proportions of 80% and 20%, respectively. A feedforward neural network

215 is trained, and we denote

$$\hat{f}_{\text{LHS}} = \hat{f}_{\theta^*} \text{ with } \theta^* = \underset{\theta}{\operatorname{argmin}} \mathcal{L}(\theta, [\mathbf{x}^{\text{LHS}}]). \quad (10)$$

216 the new estimate of f . Learning over the LHS sample is slightly less efficient than learn-
 217 ing from a single orbit dataset, as we find $R^2 = 0.9975$. This is an expected outcome,
 218 as the region covered by the learning sample is wider in the case of $[\mathbf{x}^{\text{LHS}}]$, resulting in
 219 more complex variations of f .

220 100 \hat{f}_{LHS} are trained over different learning datasets. The estimate functions then
 221 generate orbits of length 1000 MTU from 30 initial conditions that has been randomly
 222 sampled from $[\mathbf{x}^{\text{orb}}]$. The same stability criterion (Eq. 9) is applied to determine whether
 223 the \hat{f}_{LHS} orbit is stable. Contrary to orbits generated with \hat{f}_{orb} , all orbits generated with
 224 \hat{f}_{LHS} remain stable over 1000 MTUs (see Fig. 3) with $d = 4, \dots, 10$. This result sug-
 225 gests that stability can be a property of the learning sample – and not only of the type
 226 of learning algorithm or of intense tuning of hyperparameters. It also shows that extend-
 227 ing the training beyond the thin phase space region explored by a single trajectory is im-
 228 portant to improve the long-term performance (in particular stability skill) of a NN-based
 229 dynamical model.

230 However, one caveat is worth mentioning. Even though the generated trajectories
 231 are stable, in some cases, they collapse onto a fixed point near the center of one of the
 232 eL63 attractors. This seems to happen more frequently as the embedding dimension d
 233 increases. It can suggest that the size of our learning sample (i.e., 10000 individuals) may
 234 not be sufficient when the embedding dimension increases. This finding could motivate
 235 further research on how to improve the design of the learning sample in such problems.

236 5 Conclusion and discussion

237 We have developed an extended version of the Lorenz'63 model by embedding this
 238 model into higher dimension d . This new model is called the embedded Lorenz'63 model.
 239 Using a real trajectory (orbit) as a learning sample, simple artificial neural network can
 240 successfully learn the time derivatives $\dot{\mathbf{x}}$ of either L63 or eL63 models. However, unlike
 241 in L63, long trajectories generated by NNs are unstable in eL63. Instability is observed
 242 even with a minimal dimension increase, i.e., $d = 4$, and becomes more frequent as d
 243 increases. As a result, eL63 is a first example of low-dimension toy model for atmospheric
 244 dynamics that can be used to investigate the stability of NN-generated trajectories. In-

245 troduction of this new model is important, because previous attempts to construct a toy
246 model able to replicate instability issues have proven ineffective.

247 Using NNs of similar complexity but with a different learning sample, specifically
248 designed using a latin hypercube sample, solves the instability issue. We interpret this
249 result as follows. A typical eL63 orbit converges towards the model’s attractor very quickly,
250 leading to degeneracy – the orbit stays confined into a subspace of dimension 3. Con-
251 versely, a LHS generates points in the full eL63 space of dimension d , which allows the
252 NN to learn the restoring force playing away from the attractor. This result is impor-
253 tant, as it suggests that the design of the learning sample can largely influence the sta-
254 bility of the NN-generated trajectories. This finding also suggests that the design of the
255 learning sample might be an important and potentially overlooked step in IA-based at-
256 mospheric modelling. As opposed to this, much literature to date has focused on improv-
257 ing the learning technique in order to ensure stability.

258 An important further question is whether or not this new toy model can provide
259 helpful guidance for real-world problems, i.e., developing full-complexity atmospheric pa-
260 rameterizations based on NNs. In our view, the response is unclear at this stage, as a
261 few questions remain open. Is the real world as much degenerated as is eL63? The fact
262 that any orbit gets confined into a low-dimension subspace can mimic unknown phys-
263 ical laws. There is a growing literature on this topic. Recent studies show that NNs can-
264 not learn exact physical laws, typically inducing drifts in the generated trajectories (e.g.
265 Greydanus et al., 2019). Various learning techniques have been proposed to account for
266 such physical laws. However, the degeneracy could also result from a fast equilibrium
267 in response to restoring forces, just as assumed in eL63 – an issue which could be more
268 difficult to address, as physical knowledge is probably more difficult to incorporate in
269 this case. So, if some degeneracy is likely to happen in the real-world, its strength is not
270 well determined.

271 Could real-world application benefit from using designed learning samples rather
272 than ‘samples of opportunity’ like single orbits? The idea of building a specific learning
273 sample can be viewed as a data augmentation strategy. This technique first requires abil-
274 ity to calculate the value of f at any given location. Additionally, using a LHS strategy
275 as suggested above can be computationally demanding, especially if the dimension of \mathbf{x}

276 is large. In particular, we note that real atmospheric parameterizations involve a dimen-
 277 sion d much higher than those investigated with our toy model.

278 Acknowledgments

279 Code is made available at : <https://doi.org/10.5281/zenodo.4331711>.

280 References

- 281 Beucler, T., Pritchard, M., Rasp, S., Gentine, P., Ott, J., & Baldi, P. (2019). En-
 282 forcing analytic constraints in neural-networks emulating physical systems.
 283 *arXiv:1909.00912 [physics]*. (arXiv: 1909.00912)
- 284 Brenowitz, N. D., Beucler, T., Pritchard, M., & Bretherton, C. S. (2020). Interpret-
 285 ing and stabilizing machine-learning parametrizations of convection. *J. Atmos.*
 286 *Sci.*, 1–55. doi: 10.1175/JAS-D-20-0082.1
- 287 Brenowitz, N. D., & Bretherton, C. S. (2018). Prognostic validation of a neural net-
 288 work unified physics parameterization. *Geophysical Research Letters*, *45*(12),
 289 6289–6298. doi: 10.1029/2018GL078510
- 290 Brenowitz, N. D., & Bretherton, C. S. (2019). Spatially extended tests of a neu-
 291 ral network parametrization trained by coarse-graining. *Journal of Advances in*
 292 *Modeling Earth Systems*, *11*(8), 2728–2744. doi: 10.1029/2019MS001711
- 293 Brenowitz, N. D., Henn, B., McGibbon, J., Clark, S. K., Kwa, A., Perkins, W. A.,
 294 ... Bretherton, C. S. (2020). Machine learning climate model dynamics: offline
 295 versus online performance. *arXiv:2011.03081 [physics]*. (arXiv: 2011.03081)
- 296 Brunton, S. L., Proctor, J. L., & Kutz, J. N. (2016). Discovering governing equa-
 297 tions from data by sparse identification of nonlinear dynamical systems. *Proc*
 298 *Natl Acad Sci USA*, *113*(15), 3932–3937. doi: 10.1073/pnas.1517384113
- 299 Champion, K., Lusch, B., Kutz, J. N., & Brunton, S. L. (2019). Data-driven discov-
 300 ery of coordinates and governing equations. *Proc Natl Acad Sci USA*, *116*(45),
 301 22445–22451. doi: 10.1073/pnas.1906995116
- 302 Chattopadhyay, A., Hassanzadeh, P., & Subramanian, D. (2020). Data-driven
 303 predictions of a multiscale Lorenz 96 chaotic system using machine-learning
 304 methods: reservoir computing, artificial neural network, and long short-
 305 term memory network. *Nonlin. Processes Geophys.*, *27*(3), 373–389. doi:
 306 10.5194/npg-27-373-2020

- 307 Dueben, P. D., & Bauer, P. (2018). Challenges and design choices for global weather
308 and climate models based on machine learning. *Geosci. Model Dev.*, *11*(10),
309 3999–4009. doi: 10.5194/gmd-11-3999-2018
- 310 Gagne, D. J., Christensen, H. M., Subramanian, A. C., & Monahan, A. H. (2020).
311 Machine learning for stochastic parameterization: generative adversarial net-
312 works in the Lorenz '96 model. *Journal of Advances in Modeling Earth Sys-*
313 *tems*, *12*(3), e2019MS001896. doi: 10.1029/2019MS001896
- 314 Gentine, P., Pritchard, M., Rasp, S., Reinaudi, G., & Yacalis, G. (2018). Could
315 machine learning break the convection parameterization deadlock? *Geophysical*
316 *Research Letters*, *45*(11), 5742–5751. doi: 10.1029/2018GL078202
- 317 Greydanus, S., Dzamba, M., & Yosinski, J. (2019). Hamiltonian neural networks.
318 *arXiv:1906.01563 [cs]*. (arXiv: 1906.01563)
- 319 Lorenz, E. N. (1963). Deterministic nonperiodic flow. *Journal of the Atmospheric*
320 *Sciences*, *20*, 130–141. doi: 10.1175/1520-0469(1963)020<0130:DNF>2.0.CO;2
- 321 Lorenz, E. N. (1996). Predictability: a problem partly solved. *Proc. ECMWF Semi-*
322 *nar on Predictability, Vol. I, Reading, United Kingdom, ECMWF*, 1–18.
- 323 McKay, M. D. (1992). Latin Hypercube Sampling as a tool in uncertainty analysis
324 of computer models. *Proceedings of the 24th Conference on Winter Simulation*,
325 557–564. doi: <https://doi.org/10.1145/167293.167637>
- 326 Musielak, Z. E., & Musielak, D. E. (2009). High-dimensional chaos in dissipative
327 and driven dynamical systems. *Int. J. Bifurcation Chaos*, *19*(09), 2823–2869.
328 doi: 10.1142/S0218127409024517
- 329 O’Gorman, P. A., & Dwyer, J. G. (2018). Using machine learning to parameter-
330 ize moist convection: potential for modeling of climate, climate change, and
331 extreme events. *Journal of Advances in Modeling Earth Systems*, *10*(10),
332 2548–2563. doi: 10.1029/2018MS001351
- 333 Pan, S., & Duraisamy, K. (2018). Long-Time predictive modeling of nonlinear dy-
334 namical systems using neural networks. *Complexity*, *2018*, 1–26. doi: 10.1155/
335 2018/4801012
- 336 Pathak, J., Lu, Z., Hunt, B. R., Girvan, M., & Ott, E. (2017). Using machine
337 learning to replicate chaotic attractors and calculate Lyapunov exponents from
338 data. *Chaos*, *27*(12), 121102. doi: 10.1063/1.5010300
- 339 Rasp, S. (2020). Coupled online learning as a way to tackle instabilities

- 340 and biases in neural network parameterizations: general algorithms and
341 Lorenz 96 case study (v1.0). *Geosci. Model Dev.*, 13(5), 2185–2196. doi:
342 10.5194/gmd-13-2185-2020
- 343 Rasp, S., Pritchard, M. S., & Gentine, P. (2018). Deep learning to represent subgrid
344 processes in climate models. *PNAS*, 115(39), 9684–9689. doi: 10.1073/pnas
345 .1810286115
- 346 Scher, S., & Messori, G. (2019). Generalization properties of feed-forward neural
347 networks trained on Lorenz systems. *Nonlin. Processes Geophys.*, 26(4), 381–
348 399. doi: 10.5194/npg-26-381-2019
- 349 Yuval, J., & O’Gorman, P. A. (2020). Stable machine-learning parameterization of
350 subgrid processes for climate modeling at a range of resolutions. *Nat Commun*,
351 11(1), 3295. doi: 10.1038/s41467-020-17142-3

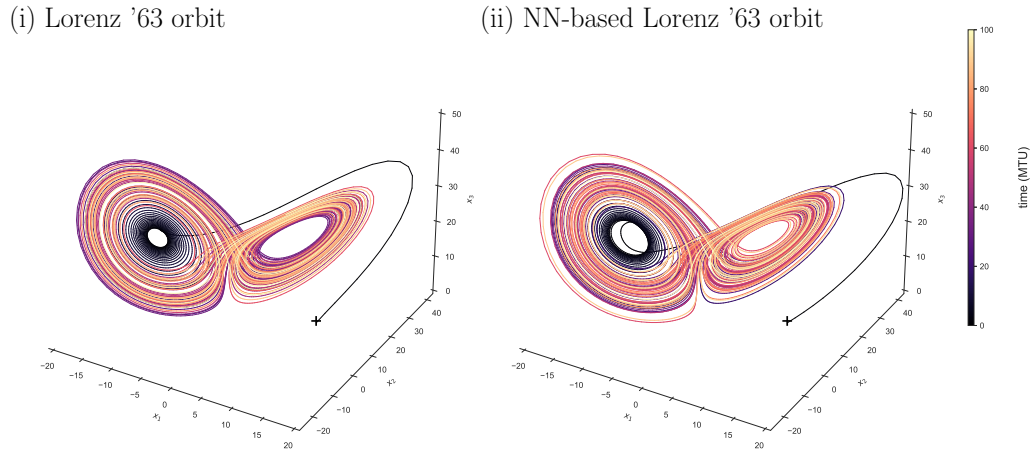
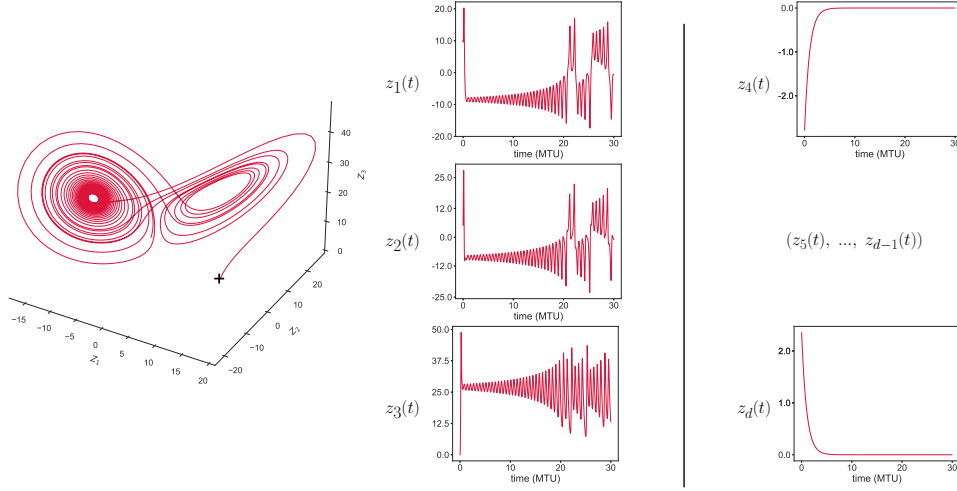


Figure 1. Examples of Lorenz'63 orbits. (i) The orbit is obtained by integration of Lorenz'63 system of equations (see Eq. 1 in the text) with $\sigma=10$, $\rho=28$ and $\beta=8/3$. (ii) The orbit results from the integration of neural network model \hat{f} (see Eq. 3). The numerical integration is performed over 100 model time units from initial condition $(10, 15, 0)$. The orbits are colored by the time variable.

(i) Embedding : $\mathbb{R}^3 \mapsto \mathbb{R}^d$

$$(z_1(t), z_2(t), z_3(t)) \mapsto \mathbf{Z}(t) = (z_1(t), z_2(t), z_3(t), \dots, z_d(t))$$



(ii) Random rotation : $\mathbb{R}^d \mapsto \mathbb{R}^d$

$$\mathbf{X}(t) = (x_1(t), x_2(t), x_3(t), \dots, x_d(t)) = P\mathbf{Z}(t), \quad P \in \mathbb{R}^{d \times d}$$

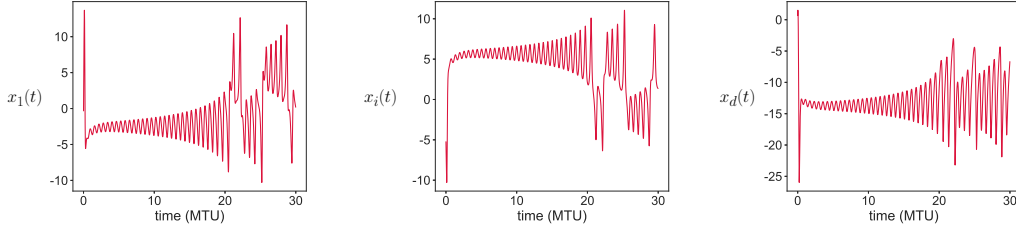


Figure 2. The embedded Lorenz'63 model (see text for details). (i) Representation of an eL63 orbit in \mathcal{B}_z basis over 30 MTU : (left) tri-dimensional representation of $(z_1(t), z_2(t), z_3(t))$, (middle) time series of $z_1(t)$, $z_2(t)$, and $z_3(t)$, (right) time series of $z_4(t)$ and $z_d(t)$. (ii) Representation of the same eL63 orbit in \mathcal{B}_x basis. Time series of $x_1(t)$, $x_i(t)$ and $x_d(t)$ are shown.

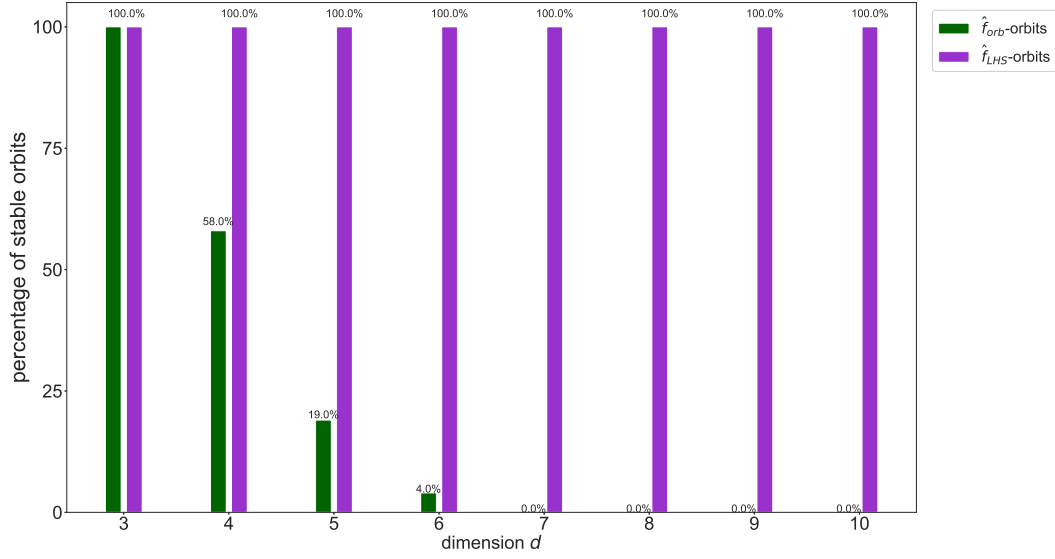
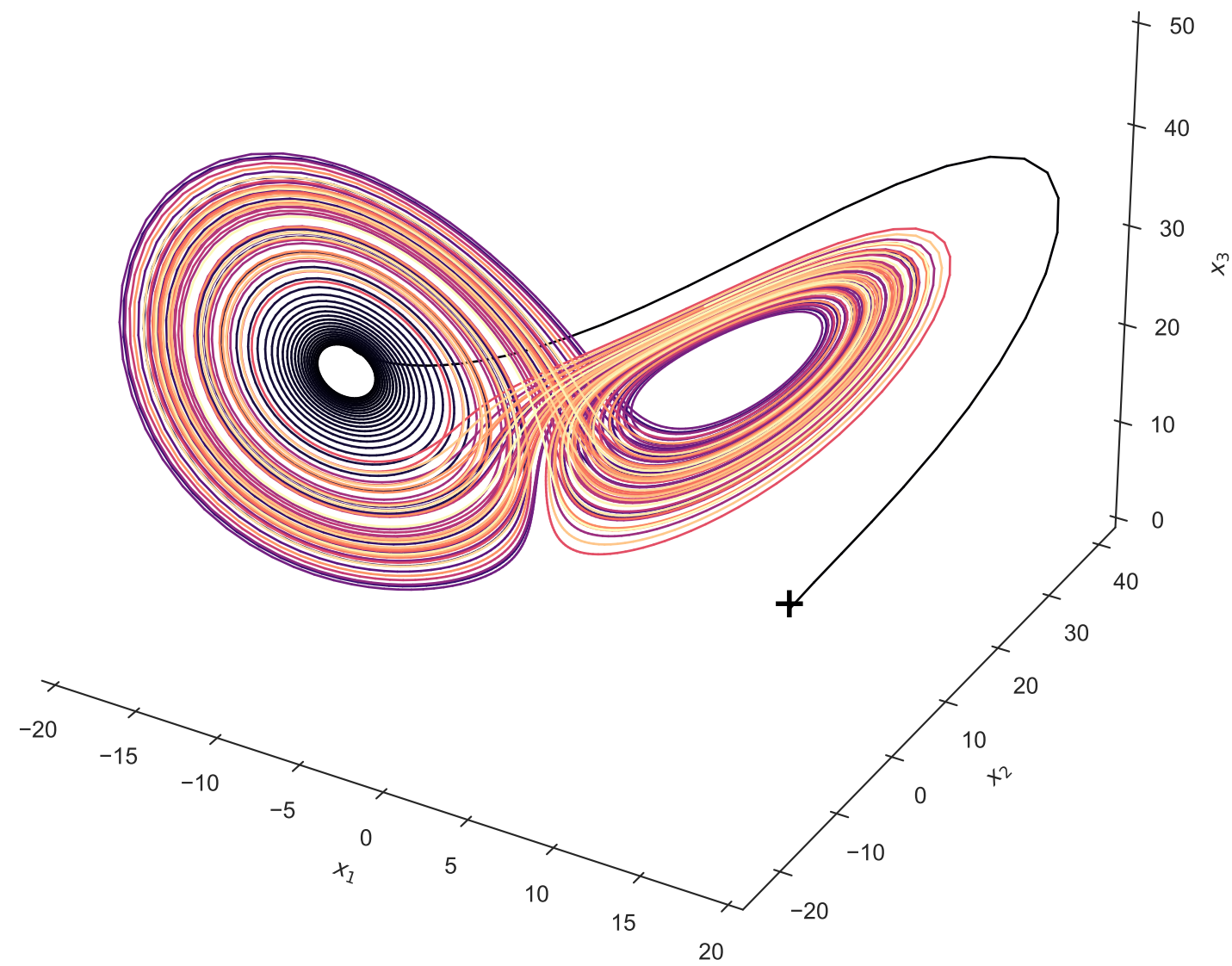


Figure 3. Percentage of stable orbits generated with \hat{f} when trained with orbital (\hat{f}_{orb} , green) or LHS (\hat{f}_{LHS} , purple) learning samples, as a function of embedding dimension d . Initial conditions are randomly sampled either in an eL63 orbit or in a region around the eL63 attractor. Stability is assessed with 100 different \hat{f} and 30 initial conditions for $d \in \{3, 4, 5, 6, 7, 8, 9, 10\}$, using the stability criterion defined in Eq. (9).

Figure 1.

(i) Lorenz '63 orbit



(ii) NN-based Lorenz '63 orbit

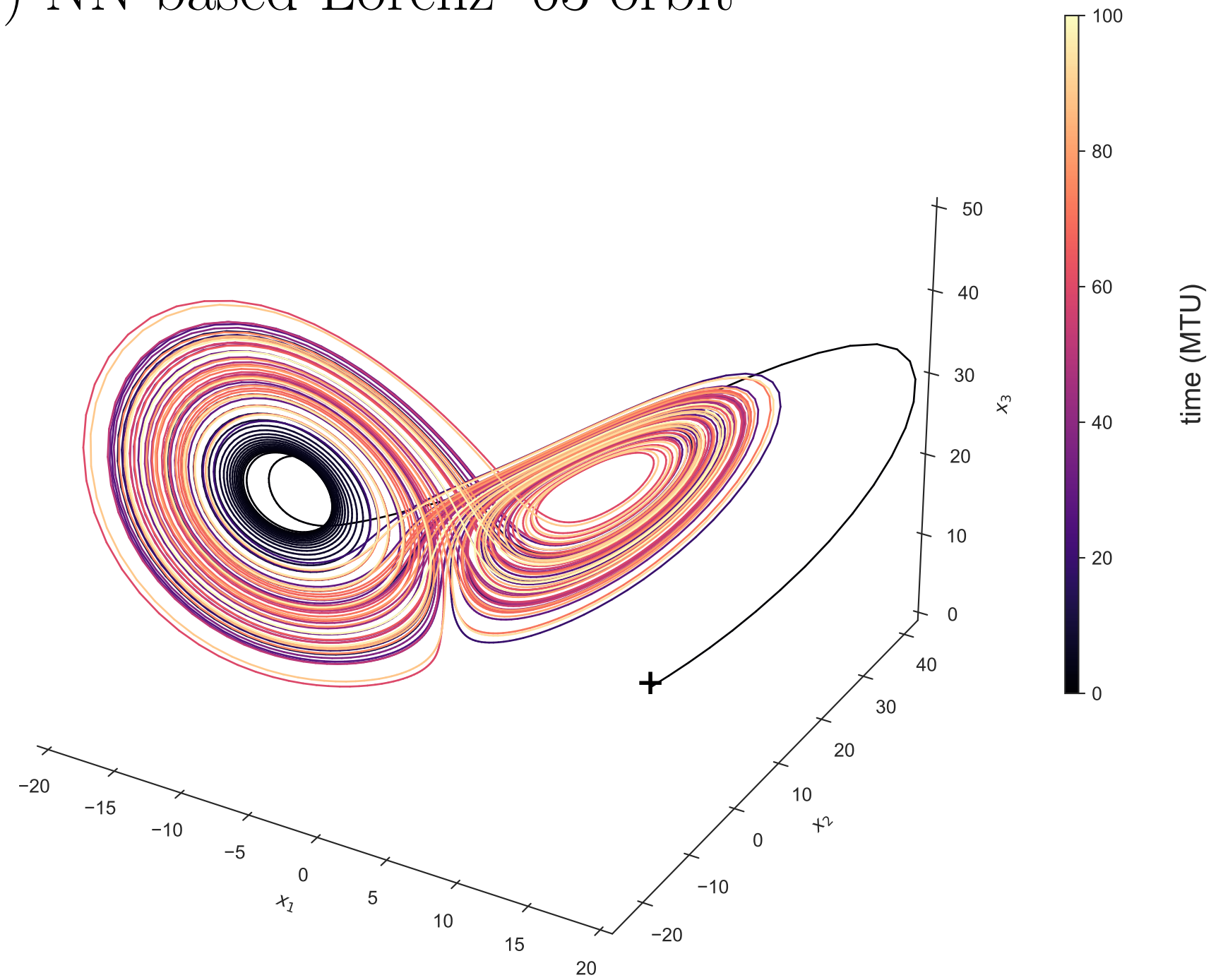
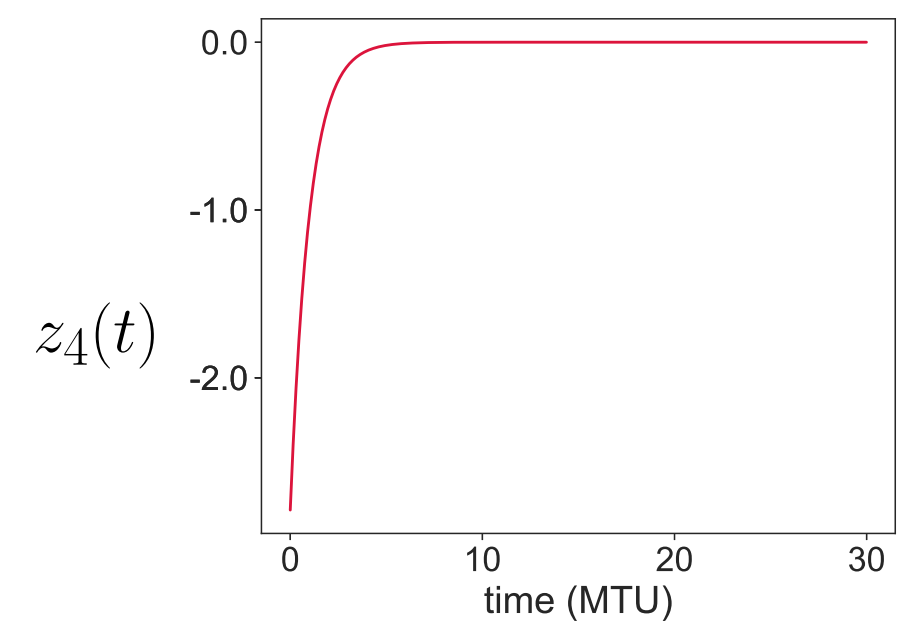
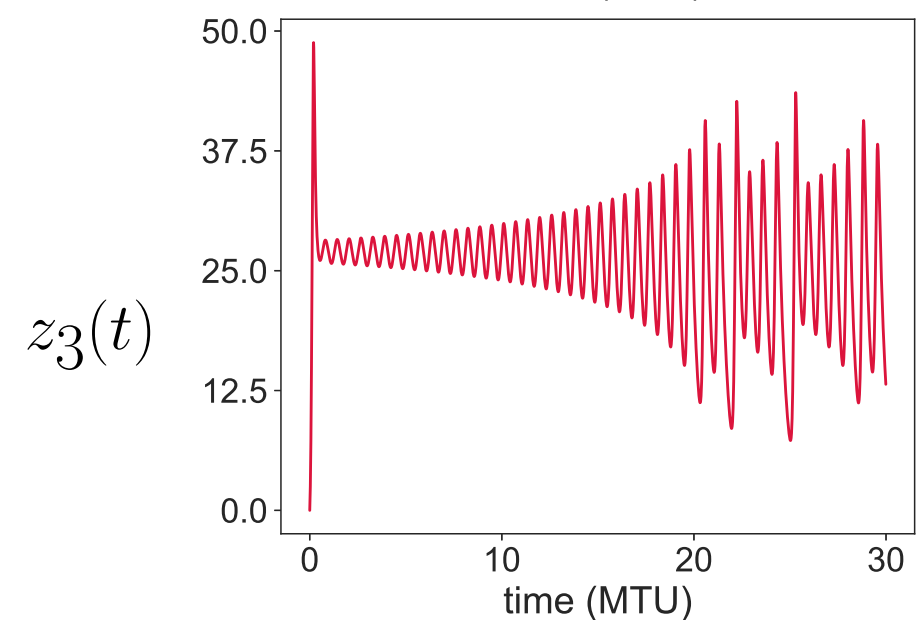
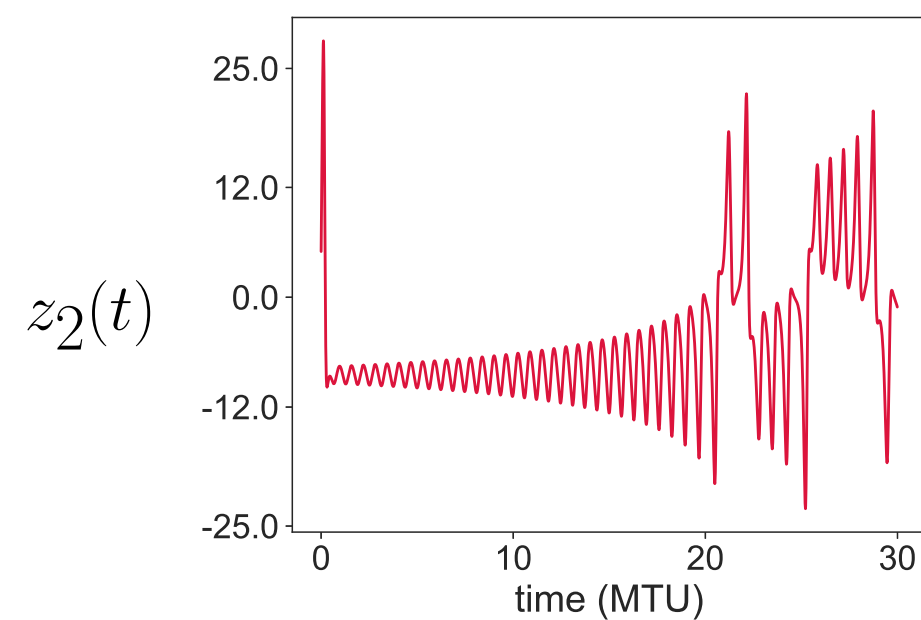
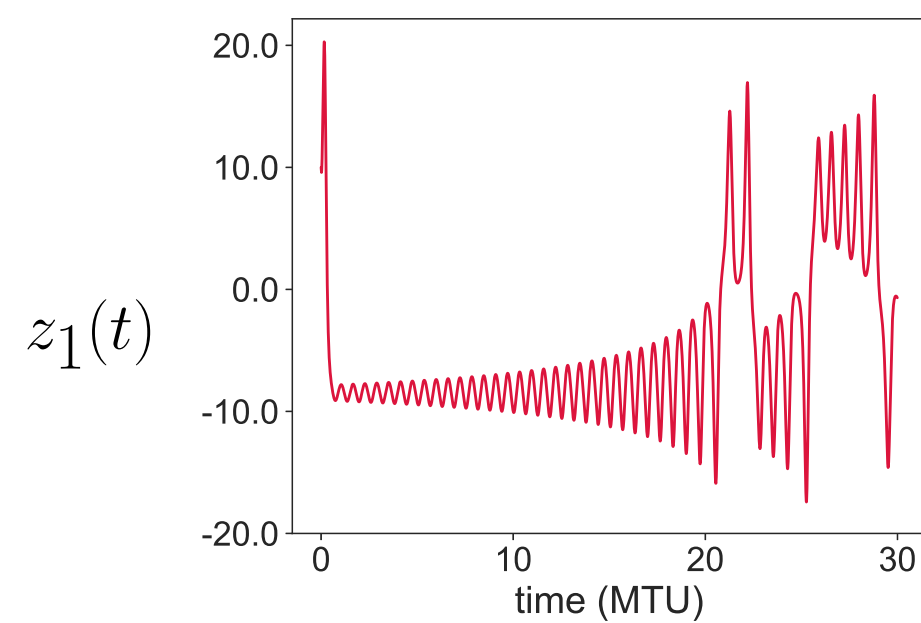
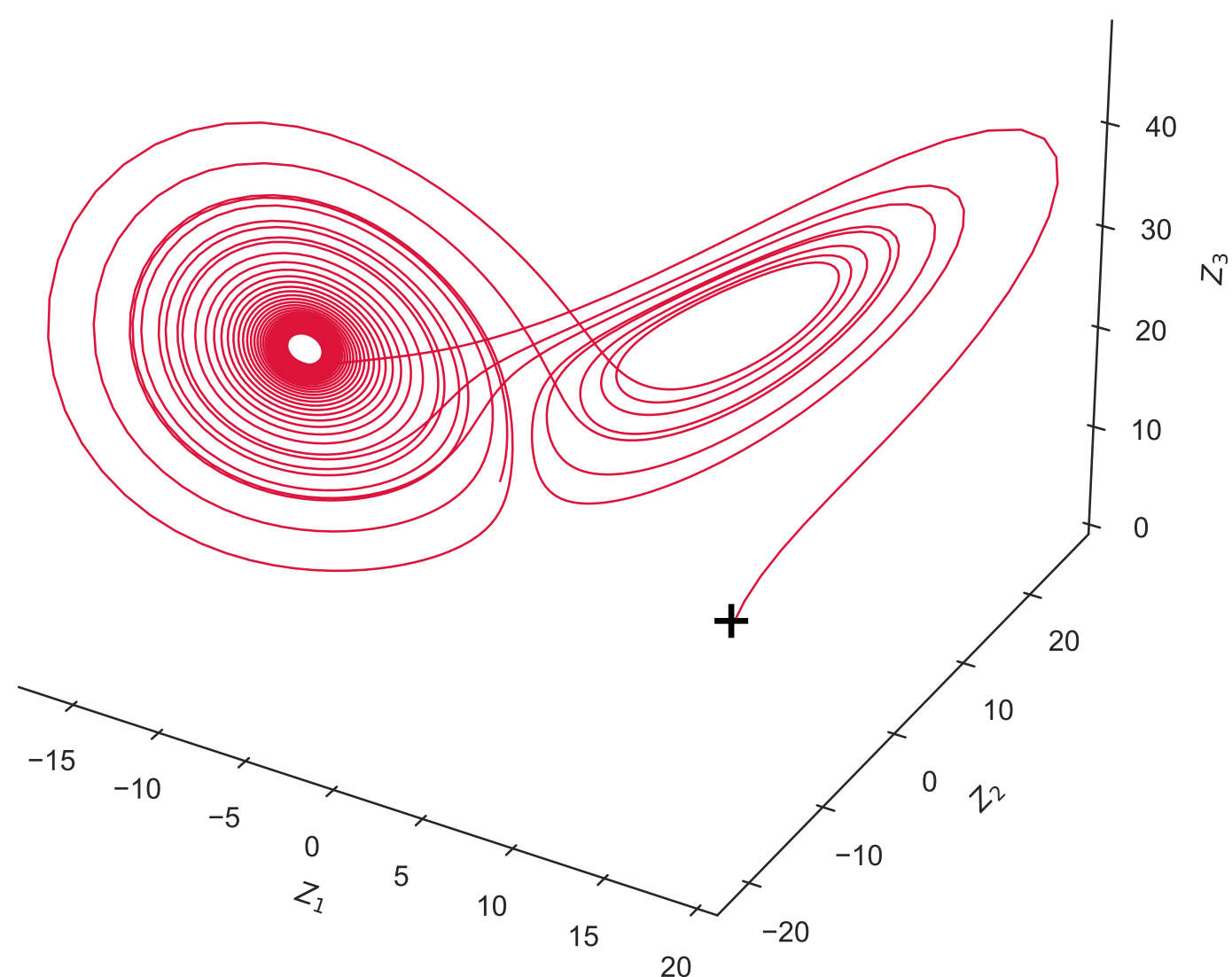


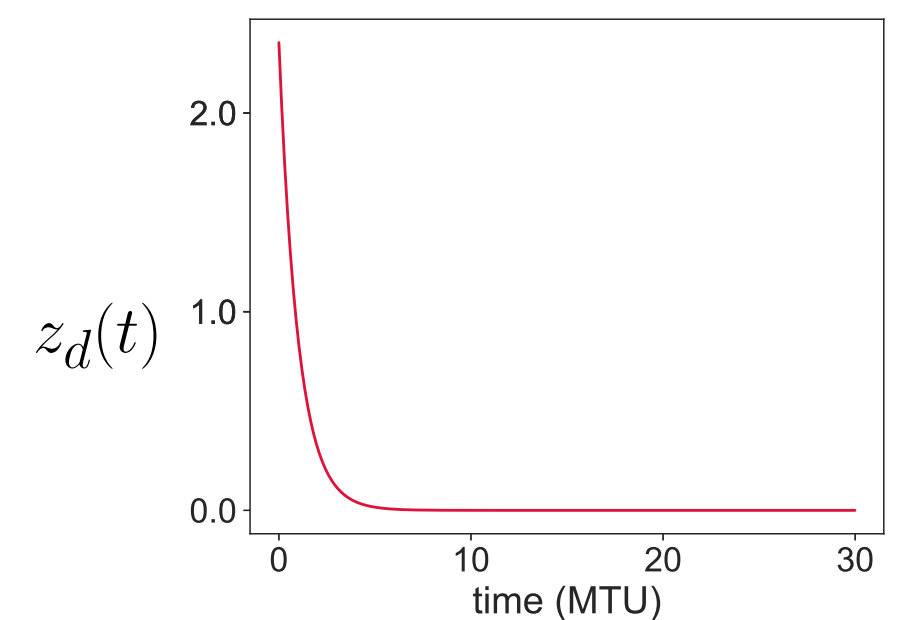
Figure 2.

(i) Embedding : $\mathbb{R}^3 \mapsto \mathbb{R}^d$

$$(z_1(t), z_2(t), z_3(t)) \mapsto \mathbf{Z}(t) = (z_1(t), z_2(t), z_3(t), \dots, z_d(t))$$



$(z_5(t), \dots, z_{d-1}(t))$



(ii) Random rotation : $\mathbb{R}^d \mapsto \mathbb{R}^d$

$$\mathbf{X}(t) = (x_1(t), x_2(t), x_3(t), \dots, x_d(t)) = P\mathbf{Z}(t), \quad P \in \mathbb{R}^{d \times d}$$

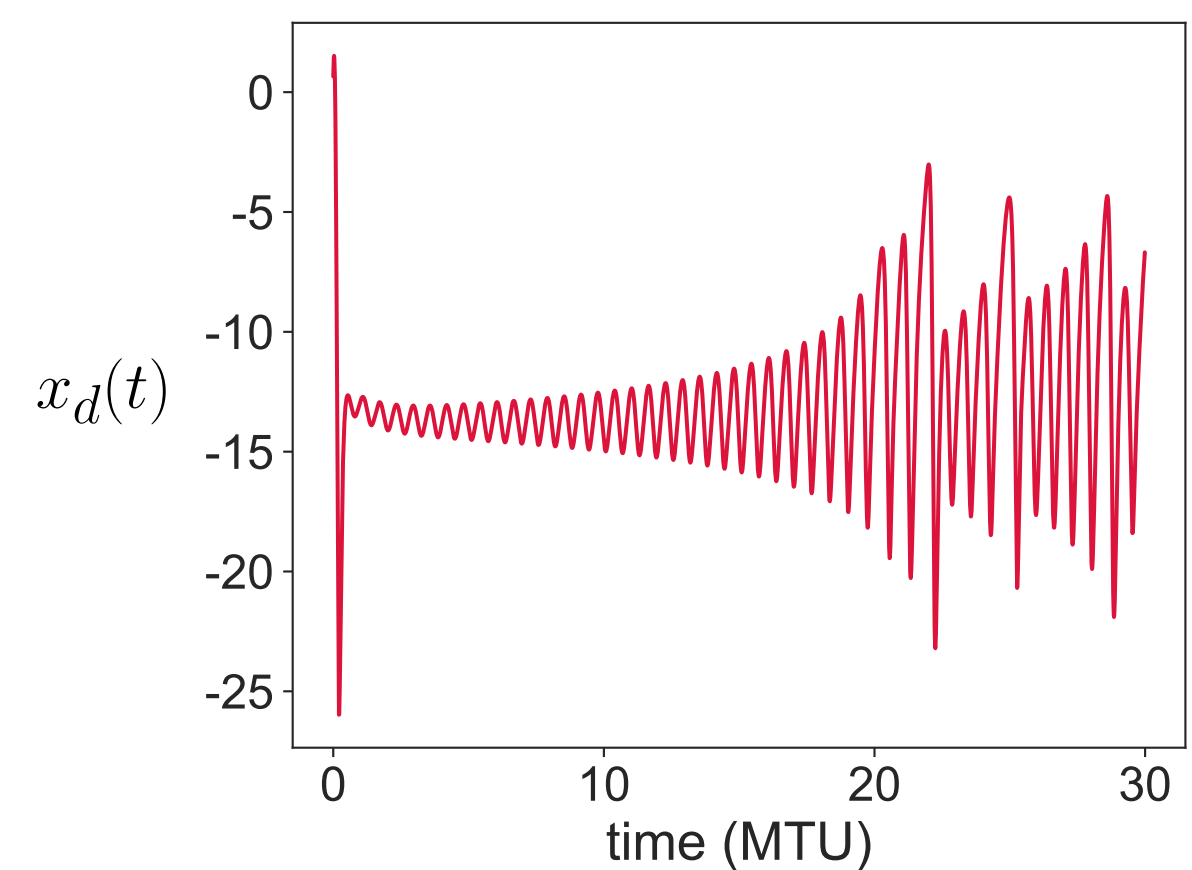
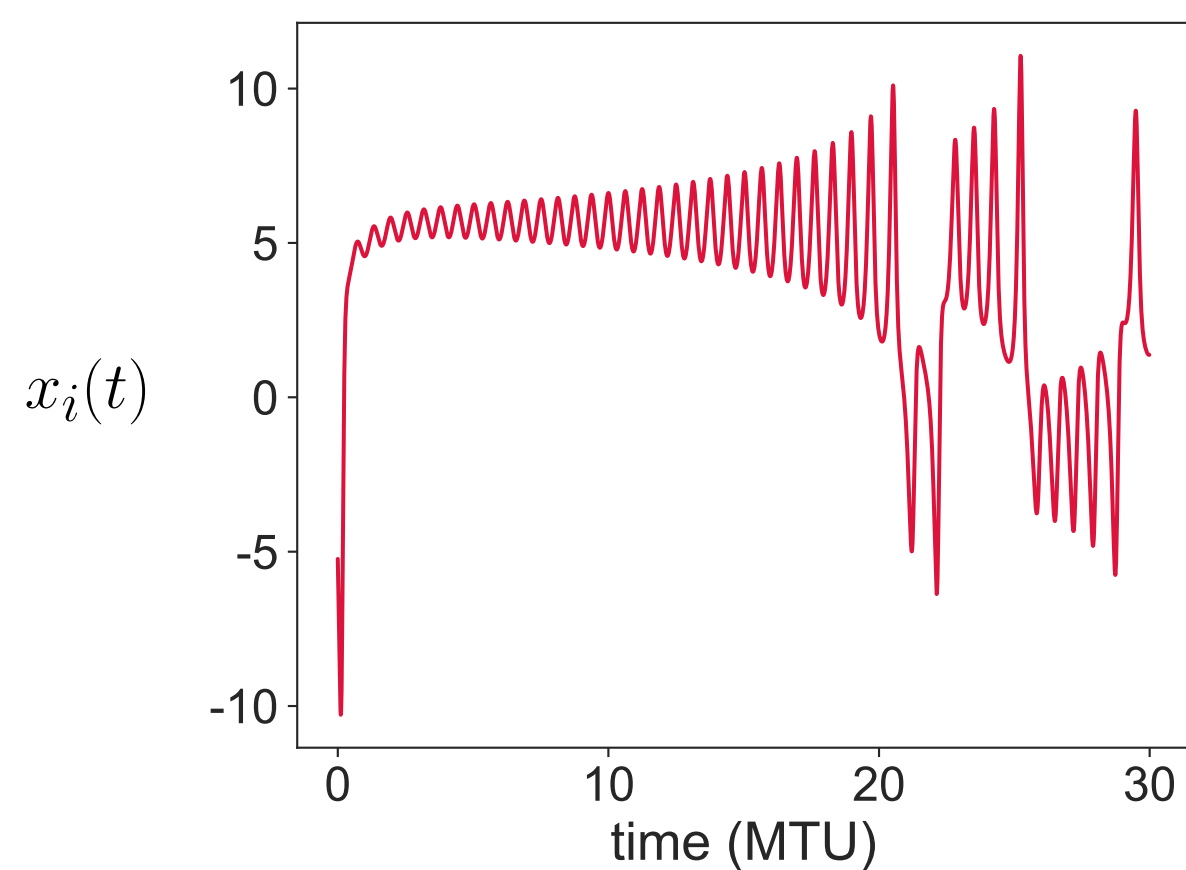
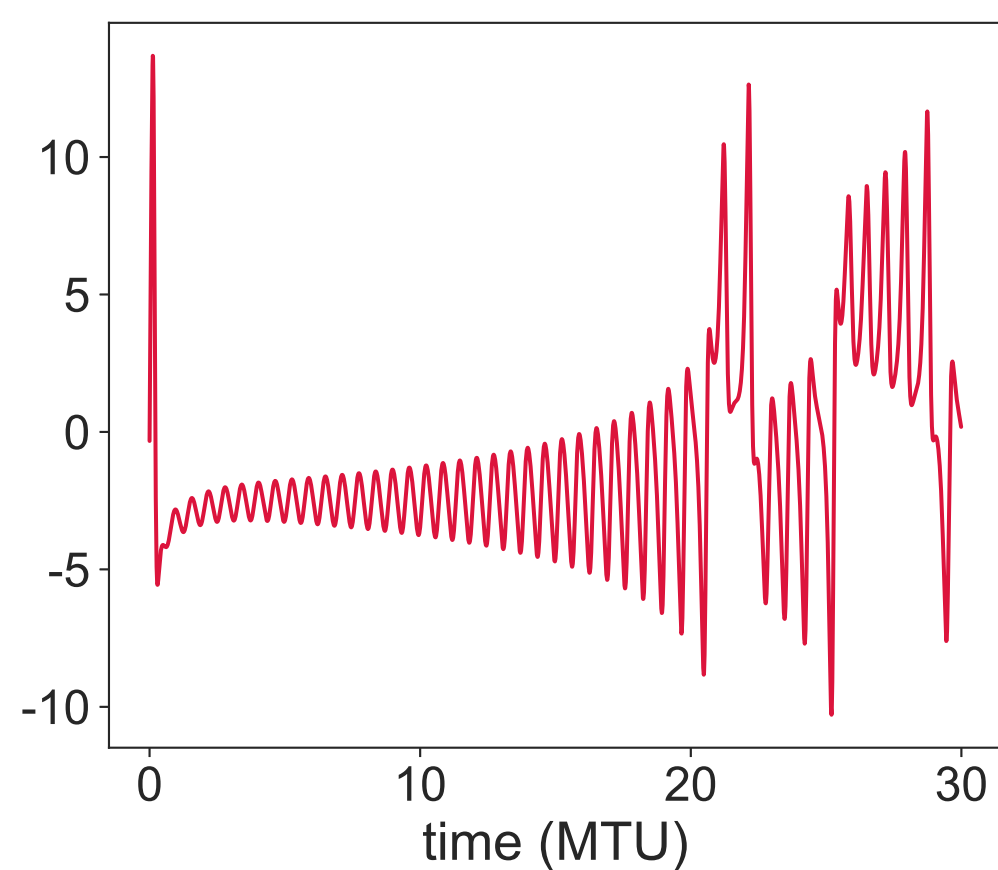


Figure 3.

